

GT-2002-30353

IMPROVING 3D FLOW CHARACTERISTICS IN A MULTISTAGE LP TURBINE BY MEANS
OF ENDWALL CONTOURING AND AIRFOIL DESIGN MODIFICATION
PART 2: NUMERICAL SIMULATION AND ANALYSIS

Jochen Gier * Sabine Ardey *

Stefan Eymann **

Ulf Reinmüller # Reinhard Niehuis #

* MTU Aero Engines, Germany

** Institute of Aeronautical Propulsion, University of Stuttgart, Germany

Institute of Jet Propulsion and Turbomachinery, RWTH Aachen, Germany

ABSTRACT

Endwall losses contribute significantly to the overall losses in modern turbomachinery, especially when aerodynamic airfoil load and pressure ratios are increased. Hence, reducing the extend and intensity of the secondary flow structures helps to enhance overall efficiency. This work will focus on secondary flow reduction in typical aero engine low pressure turbines. From the large range of viable approaches, a promising combination of axis symmetric endwall contouring and 3D airfoil thickening was chosen. Aerodynamic design, experimental verification and further analysis based on numerical simulation are described in a two part paper.

In the second part the implications of the 3D modifications on the flow structure are analyzed by employing a 3D Navier-Stokes simulation based on the experimental data reported in part one. For obtaining reliable flow simulations at typical LP turbine conditions, it is important to apply a 3D Navier-Stokes solver with proven turbulence and transition modeling to the three-stage LP turbine of the Institute of Aeronautical Propulsion at Stuttgart University.

Numerical and experimental results exhibit regions, where the modified design leads to a change in flow pattern in accordance with the design intent, as well as regions with an actual increase in loss production. The flow changes in both regions are evaluated and discussed. It is found that a certain local loss increase phenomenon can also be found in other LP turbine rigs. The reasons for this behavior are analyzed by a comparison with data from other turbine rigs and by an additional variation of the 3D design of the first stage of the investigated turbine.

NOMENCLATURE

C_{e2}, C_{μ}	[-]	constants
c	[m/s]	velocity
h/l	[-]	airfoil aspect ratio
k	[m ² /s ²]	turbulent kinetic energy
Ma	[-]	Mach number
x/b	[-]	relative axial chord
y	[m]	wall distance
α	[°]	flow angle
μ	[Pa s]	dynamic viscosity
μ_{eff}	[Pa s]	$\mu_{laminar} + \mu_{turbulent}$
η	[-]	efficiency
ω	[1/s]	specific turbulence dissipation
ζ_v	[-]	total pressure loss coefficient $= (h_2 - h_1)/(1/2 c^2)$

Subscripts

abs	absolute
t	total
w	wall
0	inlet

INTRODUCTION

In the design of modern aero engines low total operating cost is one of the main targets. Concerning turbine components this leads to a reduction (of the number) of turbine blades in a row to reduce production and maintenance cost. But this increases the airfoil load and thus has a possibly negative impact on the aerodynamic performance. In modern low pressure turbines the losses in conjunction with secondary flow development are significant and are even growing with increasing the aerodynamic load of the blading.

Multiple investigations on the development of secondary flows have been performed since the 1950's but only a part of them can be addressed here. Hawthorne [1] developed a classical model of secondary flow based on the assumption of the vortical structure of the incoming endwall boundary layer. Klein [2] was the first to report the presence of the suction side horseshoe vortex. Later, Langston [3] described also the pressure side horseshoe vortex in detail and developed a more complete secondary flow model.

Based on measurements and flow visualization several authors have further improved insight into these complex flow structures with partially different results. Especially the fate of the suction side horseshoe vortex is disputed. Sieverding performed several investigations [4,5] and reports the horseshoe vortex in a position above the passage vortex, which was supported by e.g. Sharma and Butler [6], while Goldstein & Spores [7] and Kawai et al. [8] describe different positions.

Especially in turbine rows with large pitch to chord ratio and consequently large aerodynamic loads secondary flows are significantly intensified through the increasing circumferential pressure gradient (Schäffer [9], Hodson and Dominy [10]). To alleviate this impairing effect on the turbine performance several methods have been investigated in the past. These can be divided into geometrical modifications (passive methods) and influencing boundary layers by local blowing air or air bleeds (active methods). Since this paper deals with passive modifications only the first class is discussed here.

One method to reduce passage vortex connected secondary flow are boundary layer fences. Prümper [11] investigated several variations with fences on the airfoils close to the endwalls and on the endwall platforms. The first variant showed a significant loss reduction. Unlike Kawai [12] he could not detect an improvement with the endwall mounted fences.

Three-dimensional airfoil modifications have been extensively investigated. Dejc [13] proposed leaned airfoils. These influence the radial pressure field and in case of airfoils leaned to the pressure side at the hub the aerodynamic load in the hub section is reduced by reducing the circumferential pressure gradient. This improves the situation at the hub but introduces increased passage vortex flow at the tip. To reduce the load at the tip in this case the airfoil lean is often converted into the other direction, resulting in so-called bow airfoils. Harrison [14] concluded from measurements that leaned and bowed airfoils redistribute losses radially without reducing them overall. Jansen and Ulm [15] also detect a radial loss redistribution but they find an integral loss reduction. Wang and Han [16] report of a performance improvement for a low aspect ratio airfoil with negative bow, i.e. increased load in the endwall regions.

Pioske and Gallus [17] performed an extensive variation of radial stacking and concluded that although an optimised bow airfoil hardly lowered the overall vane loss it reduced the radial flow variation downstream of that vane and improved stage efficiency by 0.6 %. A similar effect as bowing the airfoil is thickening it up in the endwall region. This was investigated by Duden et al. [18] numerically and experimentally.

Another airfoil modification with respect to secondary flow optimization is changing the radial exit flow angle distribution. Haller [19] closed the airfoil near the endwall, while Denton et al. [20]

question that this is of advantage and propose opening the flow angles in the endwall region to reduce the over-underturning caused by the passage vortex system. Other modifications include airfoil skewing (Chen et al. [21]) and bulk head leading edge design for horseshoe vortex intensification (Sauer and Wolf [22]).

Besides modifying the airfoil shape the endwall contour can be used to influence pressure and velocity fields in turbine rows. Dejc [13] was the first to report on contouring the endwall shape and a lot of later investigation were based on his proposed geometries. Morris and Hoare [23] performed experiments for geometries designed according to Dejc and reported a reduction of total pressure loss close to the non-contoured endwall of 25 % for a low aspect ratio airfoil.

Kopper et al. [24] performed similar investigations for an aspect ratio of $h/l = 0.5$ but they also restaggered the airfoil to keep the total load constant, which is important for a reliable back-to-back comparison. They reported an overall loss reduction of 17 % and an endwall loss reduction of 30 %. Ewen et al. [25] introduce Dejc's guidelines to a one stage axial turbine with very low aspect ratio ($h/l = 0.25$). They do not detect a very significant loss reduction in the guide vane but the stage efficiency improves by 1.5 %, which they attribute to the homogenization of the vane exit flow.

Atkins [26] uses a numerical code to design endwall modifications, which are not specifically based on Dejc et al. [13]. Also his aspect ratio is somewhat larger ($h/l \approx 1$) and the airfoil turning is about 100° instead of about 70° for most of the other investigations. He studies 7 different contours and detects considerable differences. However, no exit flow angles are reported and it is not clear, by which amount the aerodynamic load changed.

Rose [27] used non-axisymmetric endwall contouring to equalize the endwall pressure field. This was done with respect to endwall film cooling. In addition to pure airfoil modifications Duden et al. [18] combined 3D airfoil design with endwall contouring for a high turning low pressure turbine airfoil. Unlike many other approaches he kept overall airfoil load as well as inlet and outlet endwall dimensions constant. He employed 3D Euler and Navier-Stokes codes for studying different designs and performed measurements in a linear cascade for two modifications. Total pressure loss reduction turned out to be only small but the flow field was considerably homogenized.

Most of the secondary flow investigations so far have been performed for cascades or at the most for single stage configurations. A lot of them focussed on low aspect ratio airfoils with sometimes interacting hub and tip passage vortex systems. In the present work the investigated setup is a configuration typical for aero engine low pressure turbines with large aspect ratio, distinct secondary flow regions, high airfoil turning and steep, divergent flow duct. While in the first part of this paper the focus lies on the experimental setup and investigations, this part primarily deals with analysis based on numerical 3D Navier-Stokes simulation.

NUMERICAL METHOD

The simulations are performed with the TRACE_S 3D compressible Navier-Stokes code, which is based on a block-structured finite volume scheme. The code computes the multiple rows fully coupled. Time integration for this investigation is done using an implicit procedure. The convective fluxes are computed with higher order MUSCL scheme combined with the flux differencing method of

Roe. Fluxes are limited with a special version of the Van Albada Limiter.

The stage coupling is based on the mixing plane technique with no-reflecting boundary interfaces, flux averaging and full mass conservation. For reduction of computation and turnover times the code is vectorised and able to use shared memory parallelisation (SMP) as well as distributed memory parallelisation. More information about the numerical details can be found in Fritsch et al. [28].

Turbulence Modeling

The investigated turbine operates at Reynolds numbers typical for jet engine conditions. Thus a reliable representation of turbulence in the boundary layers is important. Therefore, the Wilcox $k-\omega$ [29] two-equation model in low-Reynolds version was employed with extensions for compressibility and system rotation.

The equations are time-discretized by 2 x 2 block-implicit time stepping. The resulting system of equations is solved with a red-black Gauss-Seidel iteration technique. For more details please also refer to Gier et al. [30].

Transition Modeling

In principle low-Re two-equation turbulence models are capable of simulating by-pass transition. However, not only a sufficient grid clustering perpendicular to the wall but also sufficient grid density in streamwise direction is needed to obtain good results. In multistage turbines the usually high free-stream turbulence level inside the passage in combination with favorable and adverse pressure gradients is further impairing a reliable transition prediction.

Therefore a transition model is employed in combination with the $k-\omega$ turbulence model for this investigation. It is based on the correlations of Abu-Ghannam and Shaw [31] with modifications of Drela [32]. It was selected from the variety of different models, because it takes the boundary layer shape and thus the pressure gradients into account. It is also dependent on the free-stream turbulence level, which is taken from the local turbulence level at the boundary layer edge provided by the turbulence model.

The transition model is applied to the entire suction surface except the leading and trailing edge, where the data of Abu-Ghannam and Shaw is not applicable, because it was gained in flat plate experiments. Due to the steady-state assumption of the computation the unsteadiness of the turbulence is averaged out in the steady-state values of turbulent energy k and dissipation ω . Since its introduction in the numerical code the transition model proved successful on various turbine configurations. Further details with additional references are given in [30] and [33].

Boundary Conditions and Computational Mesh

Non-reflecting boundary conditions are applied at inlet and outlet. Distributions of the measured total pressure, total temperature and flow angle distributions are prescribed at the inlet and static pressure at the outlet. The inlet turbulence intensity is below 1 % which is lower than in a real engine because of the specific test rig configuration.

At solid walls velocities are set to zero except for rotating walls. All walls are assumed to be adiabatic. Turbulent kinetic energy is set to zero and the specific dissipation rate ω is determined according to:

$$\omega_w = \frac{6\mu_w}{(C_{\varepsilon 2} - 1) \cdot C_{\mu} \rho y_w^2} \quad (1)$$

At the endwalls, where the cavities are neglected, a fully turbulent flow regime is to be expected. Therefore, a wall function according to Spalding is employed here, enabling the use of a somewhat coarser endwall grid resolution without a significant loss in accuracy and thus reducing the computational effort noticeably.

The computational mesh consists of 12 blocks. Each vane or blade is gridded with one O-type grid around the airfoil and a H-type grid for the major part of the channel. For resolving small flow features and to assure a dimensionless wall distance y^+ towards the profiles of about 1 the boundary layer grid is heavily clustered close to the surface. The resulting number of grid nodes in a row is approximately 600,000 with 65 nodes in radial and effectively 69 nodes in circumferential direction. The total number of grid nodes is about 3.6 million. This grid structure and resolution is currently used for high-end design applications with turnaround times of less than 10 hours on a NEC SX4 vectorcomputer in parallel mode. Most of the underlying computations have been performed on a cluster of SGI Octane workstations using the MPI version of the code. All results were accepted as converged, when massflow and efficiency of the component and the individual stages remained constant within very sharp limits and with residuals down by at least 2 orders of magnitude.

VALIDATION OF 3D SIMULATION

Before a closer look is taken into the details of the test turbine flow it is crucial to assess the quality of the flow simulation in comparison with the experimental data. All computations are based on the same inlet flow distribution, which was measured at the inlet of the transition duct (see part 1 of this paper) for the reference geometry.

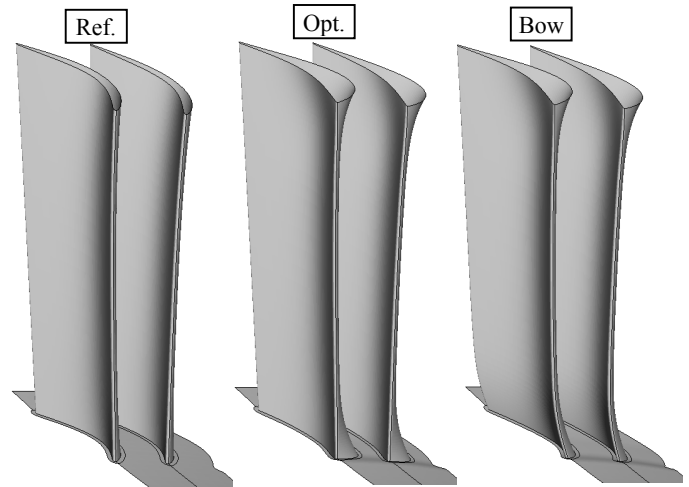


Figure 1: Comparison of reference, contoured (thickened) and bowed vane 1 airfoils

To get an impression of the geometry modification in the turbine a view of the first vane is given in figure 1 and some additional information can be obtained from table 1. More details are given in part one of the paper and in the next chapter.

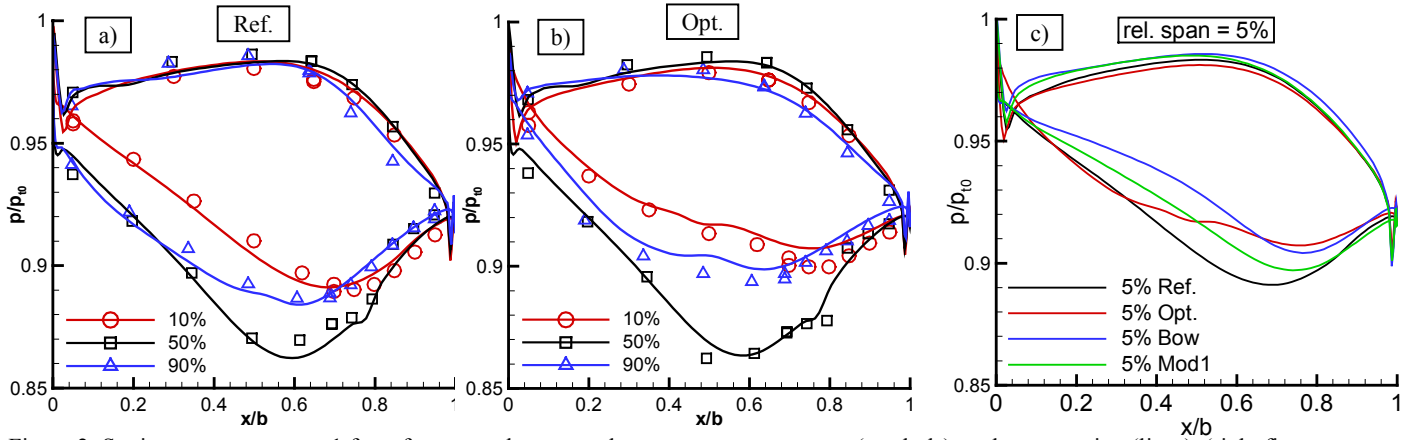


Figure 2: Static pressure on vane 1 for reference and contoured geometry, measurement (symbols) and computation (lines), (right figure computation only)

In figure 2 the static pressures on the first vane are shown at three radial positions. Generally measurement and computation correspond well. For both geometries the code is able to detect the laminar separation bubble on the suction side at midspan at 75 % axial chord. Furthermore, for the contoured build both measurement and computation exhibit a zone of little pressure gradients between 35 % and at 45 % axial chord at 10 % span. At 5 % span this zone develops into a plateau that corresponds to an additional local separation bubble vortex structure, which is discussed later in the paper.

Case	flow duct	vane 1	blade 1
Ref.	straight	constant thickness	reference
Opt.	contoured	thickened hub & tip	thickened hub & tip
Mod1	contoured	tip thick, hub thin	tip thick, hub thin
Bow	contoured	tip thick, hub thin + bow	tip thick, hub thin

Table 1: Investigated geometry variants

In figure 3 the radial distribution of the swirl angle downstream of the first vane is plotted. Both the reference geometry (Ref.) and the contoured geometry (Opt.) computations are compared with experimental data taken from the pneumatic probes. The general behavior of the flow with increasing swirl for larger radii is very well matched by the computation. Also the over- and underturning of the flow in the secondary flow regions close to the endwalls is captured. At midspan both airfoils have the identical design, which results in identical flow angles in the computation. The slight differences in the measured values for the two airfoils can probably be attributed to measurement accuracy and hardware deviations.

A comparison of the total pressure in the same plane as the swirl angles downstream of the vane 1 trailing edge is shown in figure 4. Between 30 % and 80 % span both computations exhibit identical total pressure. This means that in this range the computed loss generation is not significantly influenced by the airfoil changes in the endwall proximity. This is supported by the measured values.

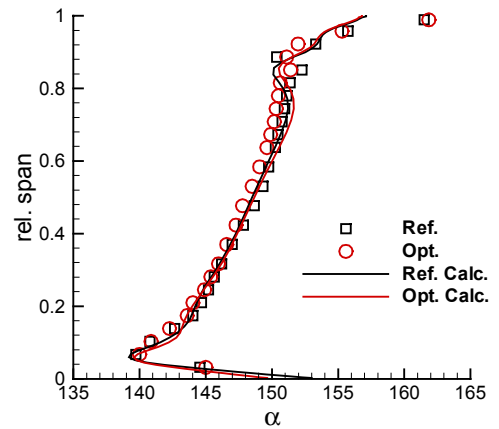


Figure 3: Swirl angle α at exit vane 1 for reference and contoured geometry, measurement (5-hole probes, symbols) and computation

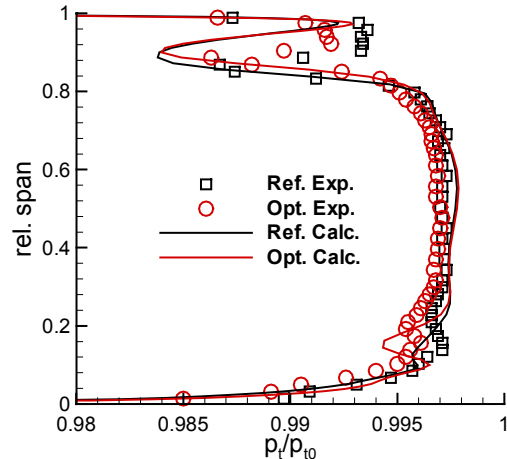


Figure 4: Non-dimensionalized total pressure at exit vane 1 for reference and contoured geometry, measurement (5-hole probes, symbols) and computation (lines)

In the casing region both the measured and the computed total pressure distributions show the typical passage vortex induced shape with a local total pressure minimum at about 90 % span and elevated

pressure at about 95 % span. The measured data has a kind of small plateau at 95 % span, which is not reproduced by the simulation. This can at least partly be due the fact that the spatial resolution of the measured inlet data is not fully sufficient to model the correct momentum thickness of the incoming boundary layer.

However, the change of the total pressure distribution at the tip, which occurs primarily due to the reduction of the radial extend of the secondary flow region for the contoured geometry, is well captured by the computation. This is an important feature for analytically comparing geometry modifications. The level of the measured total pressure in the endwall proximity is somewhat smaller for the contoured geometry, which is not seen in the computation. This is due to the fact that in the measurement also the total pressure at the inlet close to the endwalls is reduced somewhat, while the computations use identical inlet conditions for better comparability of the different variants.

Between 0 and 30 % span, thus in the proximity to the hub the computed distribution for the reference geometry shows a very reasonable match with the experimental data, although the boundary layer thickness seems to be slightly too thin. The total pressure distribution for the contoured geometry (Opt.) is characterized by a significant drop between 15 % and 20 % span also found in the calculation. This is an important feature, which will be discussed in more detail later in the paper.

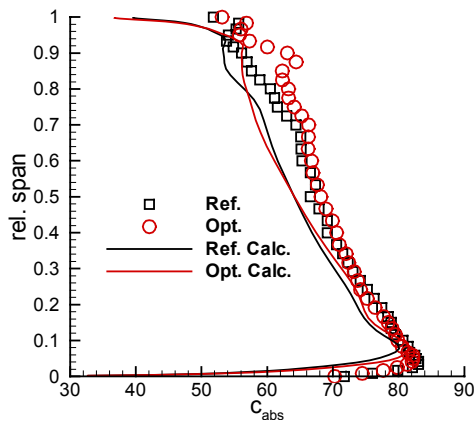


Figure 5: Absolute velocity at exit blade 1 for reference and contoured geometry, measurement (hot wire, symbols) and computation (lines)

Since the accuracy of the pneumatic probes is somewhat decreased in the measuring plane downstream of the blade 1 trailing edge due to the wake interaction hot wire measurements are taken as reference for the simulation quality. In figure 5 the absolute velocity is displayed. Overall agreement is fairly good. Especially interesting is the zone of constant velocity (zero radial gradient) at 80 – 90 % span of the contoured geometry in comparison to the reference geometry, that is also clearly predicted by the simulation.

IMPACT OF CONTOURED GEOMETRY

As described in the first part paper two modifications have been introduced in the contoured (optimized) geometry in order to reduce secondary flows, especially the passage vortex system. The airfoils of first guide vane and first rotor blade have been thickened close to the

endwalls, keeping the rest of the airfoil identical to the reference airfoils. Vane 1 has been thickened by up to factor 2.5 (figure 1 and 6) while the rotor thickening was considerably less, because the chosen thickening should be applicable to real engines. The thickening was mostly implemented on the suction sides. Furthermore the endwalls have been axis-symmetrically contoured by enlarging the flow duct area, where the airfoils are thickened as described in part 1. The second and third stage were not changed.

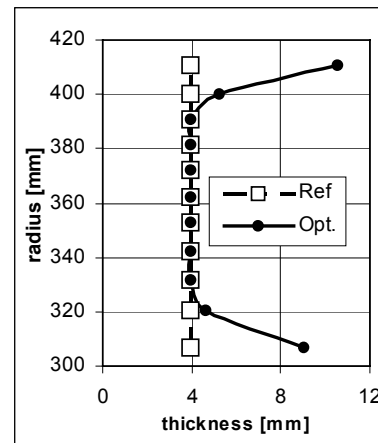


Figure 6: Thickness of vane 1, reference and contoured geometry

In figure 2 the effect of the contouring (and thickening) on the static pressure load of the airfoils can be seen. Compared to the reference vane 1 the aerodynamic load in the proximity of the endwalls has been reduced. The pressure side exhibits a somewhat decreased pressure and especially the suction side has a significantly increased pressure. At midspan the pressure load of the contoured configuration is slightly higher. This can be seen in the numerical simulation as well as in the experimental data. The maximum Mach number is slightly elevated (static pressure minimum lower) and the laminar separation bubble is a little bit more pronounced, which can be also due to small hardware deviations. Hence, in terms of profile pressure distribution the contouring modification has achieved the design intent.

The obtained reduction in circumferential pressure gradient was designed to reduce the forcing on the endwall boundary layers and thus reducing the passage vortex intensity and extension. Looking back onto figure 4, this goal is obviously achieved at the outer endwall. The total pressure is somewhat higher on average and the radial extension of the passage vortex into the mainstream is reduced.

At the inner endwall, however, instead of reducing the endwall losses the contoured configuration leads to an additional loss at about 20 % span. This effect is present in the experimental data as well as in the numerical simulation, where the effects seems to be a little more pronounced. Hence, at the hub endwall something occurs, which is different from the tip endwall region and which is also not in line with cascade data.

Computing an integral pressure loss coefficient for the first guide vane results in a net decrease of the loss, since the positive casing effect is stronger than the negative hub effect. The normalized loss coefficients are listed in table 2, where two other cases are included, which are discussed later in the paper.

	Ref.	Opt.	Mod1	Bow
Vane 1: ζ / ζ_{Ref}	1.000	0.993	0.980	1.038
Blade 1: ζ / ζ_{Ref}	1.000	1.023	1.008	0.987
$\Delta\eta_{stage1} = \eta - \eta_{Ref} [\%]$	0	0.116	0.176	-0.035

Table 2: Comparison of losses for investigated configurations

The loss coefficient of the contoured first vane is reduced by 0.7 % compared to the reference geometry loss value. However, using loss coefficients may distort differences due to the strong effect of the dynamic pressure in the denominator and therefore the stage efficiency is preferred as evaluation measure. For the first stage the efficiency of the optimized geometry raises by a delta of 0.11 %. In figure 7 the radial distribution of the isentropic efficiency of the first stage is plotted. Comparing the reference and the contoured distributions it becomes obvious that at the outer duct the contouring resulted in an improved efficiency, while at the hub efficiency was impaired. Considering these results the questions arise, what happens in the hub region and what is the impact on design optimization.

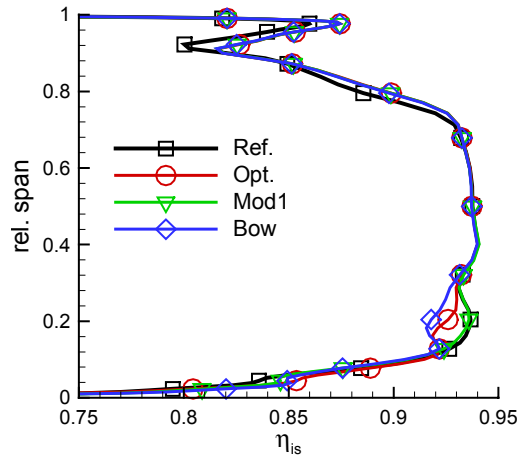


Figure 7: Radial distribution of isentropic efficiency of stage 1, comparison of investigated cases (symbols for better comparison only)

GEOMETRY VARIATION AND ANALYSIS OF INNER DUCT FLOW STRUCTURE

In addition to the two geometries experimentally investigated and discussed above, two other modifications were investigated numerically for this work. The starting point of Modification 1 (Mod1) simply was to try to regain the original performance close to the hub by omitting the airfoil thickening in vane 1 and blade 1. The duct contour of the contoured case has been retained unchanged, so the inner duct region of Modification 1 (Mod1) is not identical to the base design (Ref.).

The second modification basing on the Mod1 variant introduces a bow in the first vane hub region. The bow is leaned towards the airfoil pressure side as is customary (figure 1).

The resulting performance for these cases is listed in table 2. It can be seen that the Mod1 geometry reduces the vane 1 loss slightly more than a factor of two compared to the contoured variant (Opt.). This also results in a further improved stage efficiency. The obvious reason is, that the efficiency close to the hub assumes the same level as in the reference cases while maintaining the gain at the outer duct (figure 6).

Introducing the bow at the hub in vane 1 yields an interesting result. The loss of vane 1 is significantly increased and the worst of all 4 cases. However, the bow seems to reduce losses in the following rotor blade making up for some of the vane losses. Overall the stage efficiency drops slightly below the level of the reference case (Ref.). Obviously the bow introduces additional losses at the hub as does the airfoil thickening. In the following it will be discussed whether the problems at the hub have the same origin for both design principles, i.e. whether the concave radial stacking of the suction surface is the cause for the additional losses.

Putting the four cases together it becomes clear that having a relatively straight airfoil in the hub proximity does not show a problem and producing a concave radial stacking on the suction surface results in additional losses.

In figure 8 the total pressure distribution in the vane 1 exit plane is shown for the reference and the contoured case. At the tip the total pressure deficit area, caused by the strong passage vortex is reduced in extend and intensity for the contoured case. This is perfectly in line with the design intent and the experience from cascade tests, e.g. of Duden et al. [18].

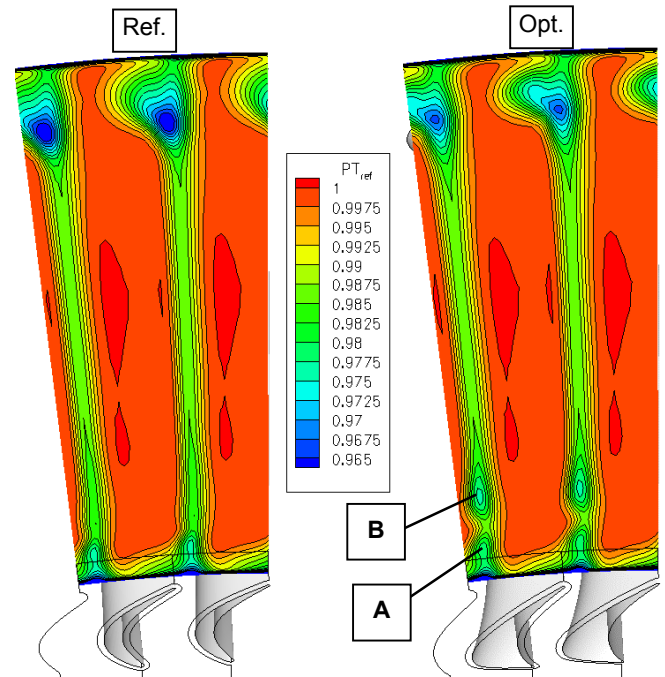


Figure 8: Total pressure pt/pt_0 downstream of vane 1 for reference and contoured case

With the reference geometry the passage vortex at the hub is only little distinct. As could be seen in figure 3, the flow angle shows the typical over- and underturning, which means that there is some secondary flow motion. In contrast to the outer duct region, this is not

strong enough to produce a significant vortex core where low energy fluid is collected. At the hub the pitch is considerably smaller than at the casing reducing the passage vortex creation forces. Also the radial pressure gradient from outer duct to inner duct in the vane causes the low momentum region of the passage vortices to move radially inwards, that is into the core flow at the outer duct and towards the endwall for the inner duct. Consequently the Mod1 geometry, which at the hub combines a thin airfoil with a contoured flow duct, shows almost no change in endwall losses although the circumferential pressure gradient is significantly reduced by the contouring. Only a tiny improvement can be seen in figure 7 at 4 % span.

With the contoured geometry (Opt.) the passage vortex on the hub behaves similar to the reference case (Ref.) (Point A, figure 8). But there is an additional loss region B, which corresponds to the radial total pressure profile in figure 4 and is detached from the passage vortex system. Interestingly this pattern is resembled by the distribution of turbulent kinetic energy k in the same plane downstream of the vane trailing edge (figure 9).

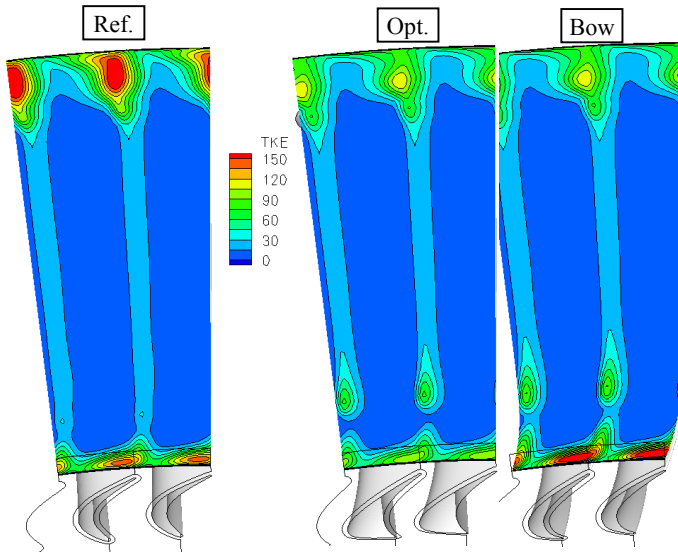


Figure 9: Turbulent kinetic energy k downstream of vane 1 for reference, contoured and bowed case

In the casing region the contouring not only results in a reduced size of the passage vortex system but also in a significantly decreased intensity of turbulence. On the hub there is a turbulent region at the same position (20 % span), where the total pressure distribution has a local minimum. This is also related to an additional vortex center (axial vorticity, figure 10). For the reference case this distribution is very similar to the measured secondary vorticity (figure 10, part 1).

In the bow case the turbulent kinetic energy very close to the hub is at about the same level as in the reference case, thus higher than in the contoured case with the thickened airfoil. In addition it shows a similar local peak at about 20 % span as the contoured version, which corresponds to a local maximum in axial vorticity. This leads to the relatively high loss parameter in the first vane for the bow airfoil.

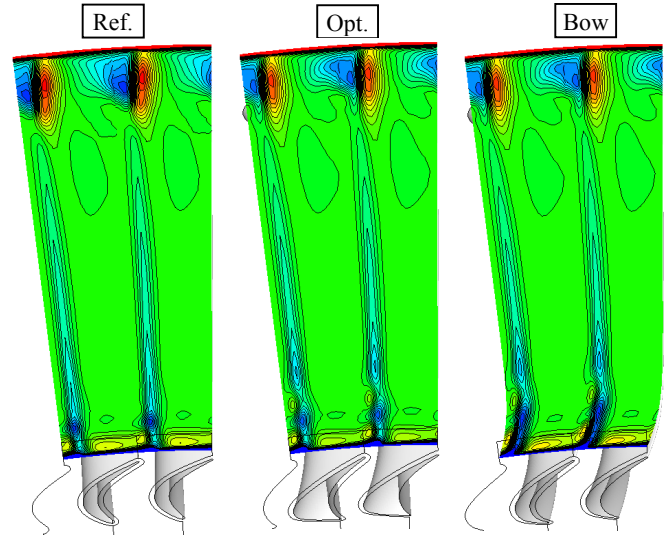


Figure 10: Axial vorticity downstream of vane 1 for reference, contoured and bowed case

To get a better insight into what is happening, streamtraces on the vane 1 airfoil are shown in figure 11. These streamlines are produced by projection of the flow vectors in the first numerical grid plane above the airfoil surface onto the airfoil surface. They thus represent the flow direction in the very proximity of the vane surface.

The streakline picture for the reference case does not show anything abnormal. At about 75 % axial chord there is a small laminar separation bubble with reattachment. At the tip the streakline pattern of the passage vortex on the suction side, which starts at approximately 50 axial chord, is typical. At the hub only a very limited passage vortex influence is visible.

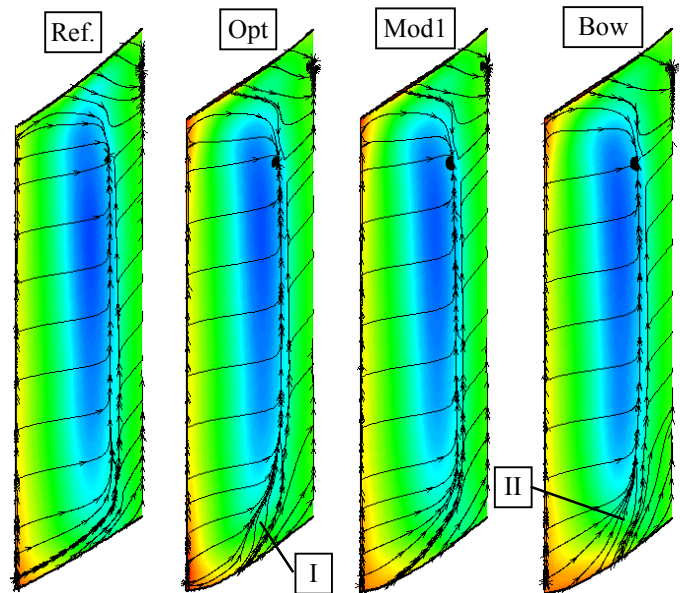


Figure 11: Static pressure and streaklines on airfoil suction surface, vane 1

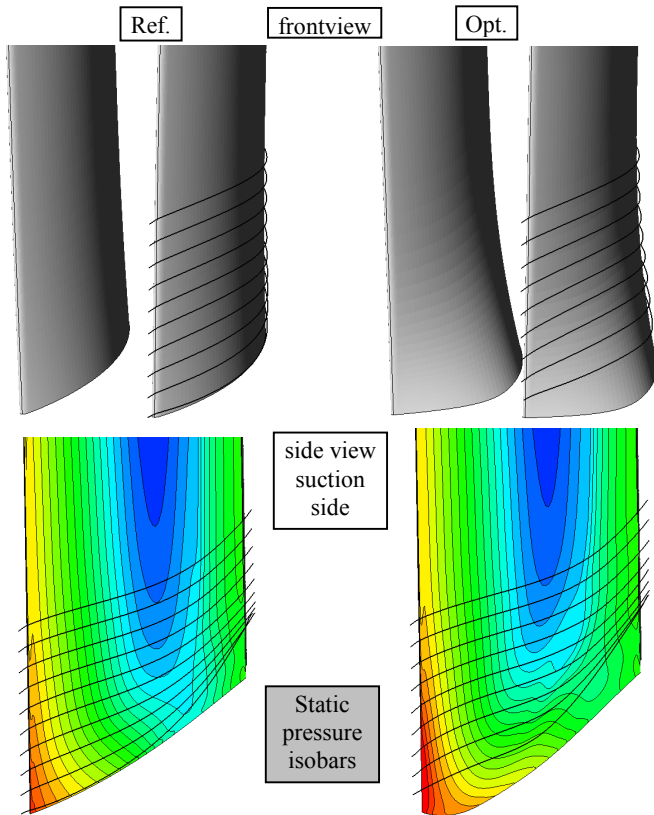


Figure 12: Streamlines on suction side in hub region, starting from leading edge outside of the boundary layer

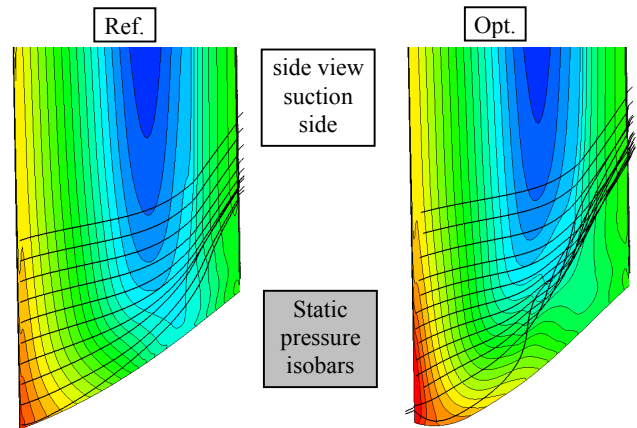


Figure 13: Streamlines on suction side in hub region, starting from leading edge inside of the boundary layer

In the contoured geometry (Opt.) the pattern at the tip does not change considerably. At the hub, however, a new vortex structure (I) appears. This vortex structure corresponds to the pressure plateau in figure 2b at 10 % span. The bow airfoils produce a somewhat different but still related pattern in area II. Comparing both modification versions with the case Mod1, which is a straight airfoil combined with contoured endwall it becomes clear, that the endwall contouring alone does not hurt the flow structure. The key to the increased loss is obviously connected to the form of the airfoil suction side.

In figure 12 the reference and the thickened airfoils are shown with three-dimensional streamlines, starting at about the leading edge close to the airfoil but *outside* the boundary layer.

The streamlines in the reference case basically remain on their spanwise location until about 50 % axial chord where the influence of the passage vortex becomes dominant. Contrary to that, the streamlines in the contoured case with the thickened airfoil are

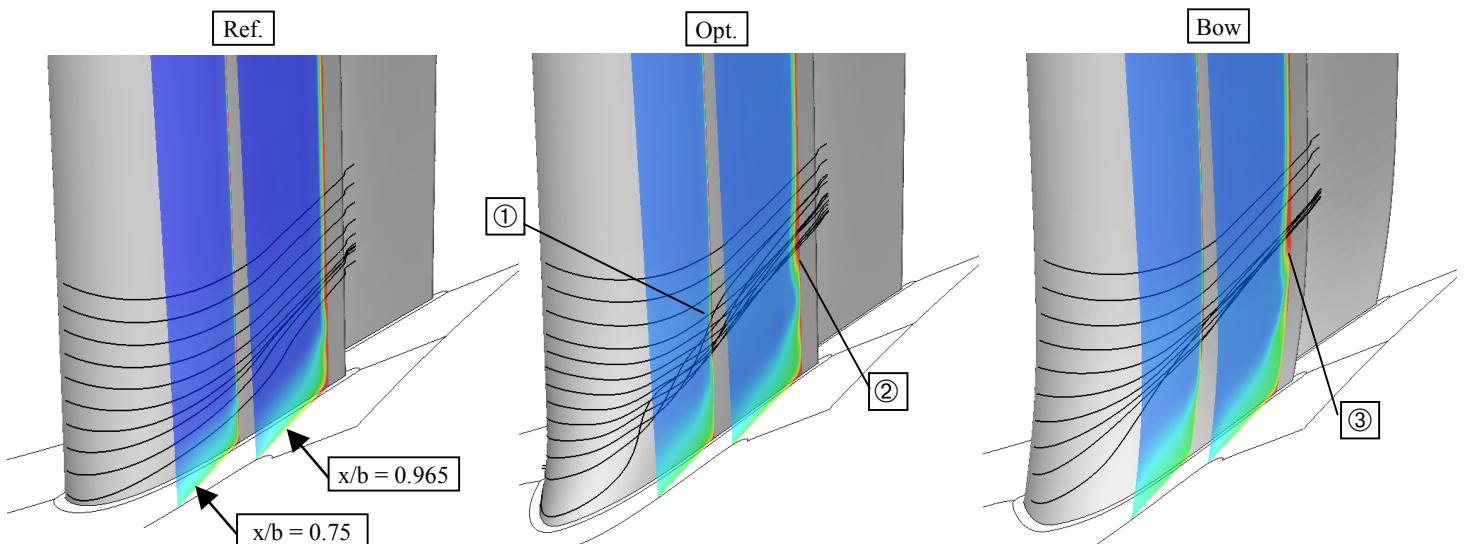


Figure 14 Streamlines and entropy contours in two axial planes located at 75 % and 96.5 % axial chord

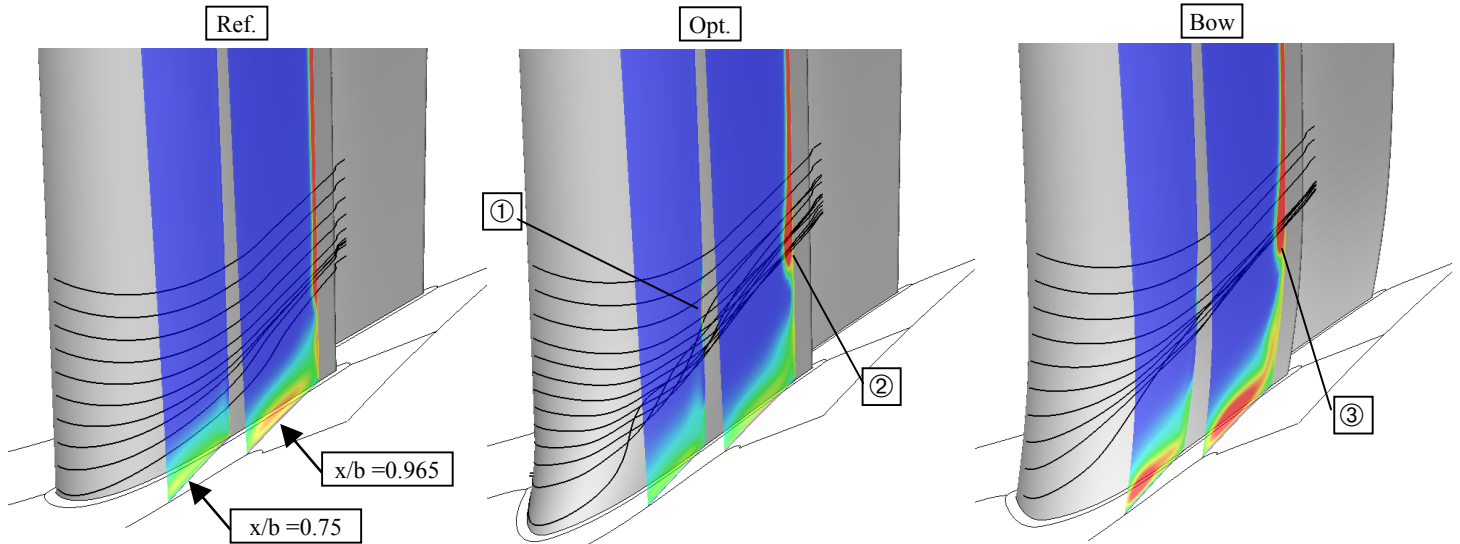


Figure 15: Streamlines and turbulent kinetic energy in two axial planes located at 75 % and 96.5 % axial chord

diverted radially outwards from the leading edge up to about 30 – 40% axial chord, where the thickening peaks. These streamlines describe a kind of great circle. For the contoured case this means that the pressure distribution in figure 2 is misleading, because here the data is plotted on constant relative channel heights. Moving on a great circle the flow close to the boundary layer starts moving radially inwards at 40 % axial chord, imposing deceleration i.e. flow against a positive pressure gradient onto the boundary layer. Since the boundary layer is still laminar here, the boundary layer flow separates and forms the additional vortex seen in position I in figure 11. It is displayed by the three-dimensional streamlines in figure 13. After its generation the vortex is driven to larger radii by the radial pressure gradient.

By looking onto the streamlines downstream of about 50 % axial chord in figures 12 and 13 it seems that the radial displacement is comparable for both cases, indicating only a moderate change in passage vortex intensity.

In figure 14 entropy contours are shown at two axial planes at 75 % and 96.5 % axial chord, respectively. The streamlines are identical to figure 13.

In area ② (plane $x/b = 96.5$) in the contoured vane a spot of increased entropy can be seen. This spot corresponds to the total pressure deficit in the plane downstream of the vane and the resulting loss increase (figure 8). This is the region, where the additional vortex mixes out. It is the source of the increased vorticity at 20 % span (figure 10). Although it is only a very thin region there is already some entropy production at $x/b = 75\%$ in position ①. This thin region is actually partly located above the vortex. The cause for the local turbulence increase in point ① is a beginning transition (figure 15). Actually transition starts locally upstream of region ① at a radial position of about 20 % span because the suction side of the thickened airfoil has a bend where the airfoil thickening is connected to the reference airfoil (see figure 6). In this bend the transition starts further upstream than on the rest of the airfoil.

The earlier transition and the additional vortex seem to interact. The upstream transition intensifies the mixing inside the vortex, leading to increased losses. Furthermore the resulting low momentum

region of the mixing vortex faces an increased boundary layer growth due to the adverse pressure gradient caused by the gradually reducing airfoil thickness downstream 40% axial chord as already explained (Fig. 12). This further enhances turbulence production. Hence, the increased loss at 20 % span downstream of the trailing edge as well as the increased vorticity and turbulence kinetic energy is primarily caused by the bend in the suction side surface and the resulting interaction of transition and suction side bend vortex.

In case of the bow the basic interaction effect seems to be similar, since the bow also reduces aerodynamic load close to the hub but increases load in the region, where the bow finally transforms into the reference airfoil shape, which is also the case at approximately 20 % span. There are some differences in detail, compared to the contoured, thickened airfoil case causing the bend vortex to be smaller but the additional turbulence and loss production is comparable.

Generally this effect of additional loss production due to suction side bend can also be expected to occur in the outer duct region, too. However, even if there is a small negative effect it is far outweighed by the positive effect of reducing the strong passage vortex associated losses.

As stated above, the passage vortex is relatively weak at the hub. This is why thickening the airfoil (like in this investigation) or giving it a suction side bow at the inner duct cannot be expected to improve the flow situation in a turbine configuration like the one investigated in this work.

COMPARISON TO OTHER TURBINES

In figure 16 results from two other three-stage turbines are displayed. They base on equivalent Navier-Stokes computations and have already partly been described in Gier et al. [30] and Gier & Ardey [33]. The left picture shows a similar view as figure 15 for the third guide vane. This airfoil has a high turning and pressure loading and was designed with moderate airfoil thickening close to the endwalls. Although the airfoil thickening is more moderate in this turbine compared to the turbine described above, it still shows similar

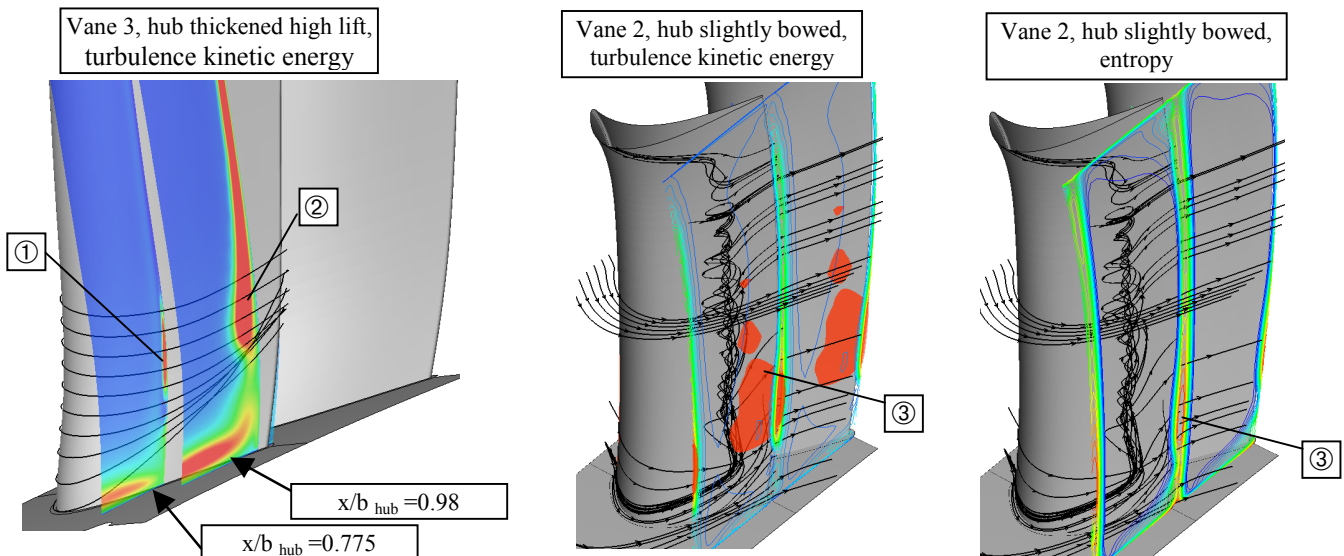


Figure 16: Streamlines, turbulent kinetic energy and entropy of two three-stage test turbine with resembling design features

features. In region ①, where the thickening is vanishing, the turbulence is already elevated compared to the surrounding regions.

In the middle and right picture the second vane of a similar turbine with normal airfoil load and a slight bow in the hub region is shown. In area ③ increased turbulence production is detected, resulting in an increased entropy level. As can be seen from the streamlines this region is actually subject to increased loss production, but it is not connected to the low momentum material collected by the passage vortex.

CONCLUSIONS

In this second part of the paper the flow in a three-stage LP turbine run at the University of Stuttgart has been investigated in detail with respect to secondary flows by the use of a modern 3D Navier-Stokes solver. The turbine is typical for jet engine design. The airfoils have a high aspect ratio and a turning of more than 80 degrees. The numerical investigations were complemented by experimental data gathered in the test turbine.

In order to assess the flow structure details and overall performance information with a high degree of quality, a reliable transition model was combined with the $k-\omega$ turbulence model. The simulations corresponded well with the experimental data.

The first guide vane and the first rotor had been redesigned to improve turbine performance through reduction of secondary flows. Therefore, endwall contouring and airfoil thickening were employed at inner and outer duct. At the tip, the redesign was successful in reducing the radial extend of the passage vortex system, reducing flow inhomogeneity and even reducing the loss close to the endwall without significantly changing the flow in the core at midspan.

At the hub, however, an additional loss region was detected in accordance with the experiment at about 20 % span. It was found that this additional loss was induced by a new vortex created on the airfoil suction side. To ascertain which design feature can be made responsible for this unwanted loss increase, a bow was designed for

the hub instead of the thickening, because the bow features a similar suction side stacking. The bow actually showed similar suction side loss behavior. By comparing the flow phenomena of the thickened and bowed hub designs to an airfoil without any 3D feature but still the same endwall contouring at the hub, it became clear that the endwall contouring did not harm the turbine performance.

Both experimental and numerical approaches showed that it is possible to reduce secondary flow motion in this type of turbine with the chosen measures and that this is especially promising in the casing region. Judging the success of such measures experimentally proved difficult and employing numerical simulation helped in complementing the conclusions and in gaining a deeper insight into the physical mechanisms.

Finally it is concluded that if the passage vortex is relatively weak – as it is the case at the hub of turbines of this kind – any geometry modification has little effect on the secondary flow. Hence, the negative impact of the chosen airfoil modifications occurring in conjunction with the suction side flow has a significant effect. If the passage vortex is strong – as in the casing region – the loss reducing effect of the 3D design on the secondary flow is significantly larger than its negative effect in conjunction with the suction side flow.

These implications should be taken into account in the design of turbines with similar geometrical characteristics. Especially at the inner duct three-dimensional airfoil design should be applied only very carefully.

ACKNOWLEDGEMENT

The work leading to the results of this paper was carried out within the German joint industrial and academic research program AG TURBO and has been supported by the German research ministry (BFMB) through contract 0327040J. The content of the publication lies in the responsibility of the authors.

REFERENCES

- [1] Hawthorne, W.R., 1955, "Some Formulae for the Calculation of Secondary Flow in Cascades", ARC-17519, Dep. of Engineering, Univ. of Cambridge
- [2] Klein, A., 1966, "Untersuchungen über den Einfluß der Zuströmungsgrenzschicht auf die Sekundärströmungen in den Beschauelungen von Axialturbinen", *Forschung im Ingenieurwesen*, Vol. 32, No. 6, pp 175-188
- [3] Langston, L.S., 1980, "Crossflows in a Turbine Cascade Passage", *ASME Paper 80-GT-5*
- [4] Sieverding, C.H., Van Den Bosche, P., 1983, "The Use of Coloured Smoke to Visualize Secondary Flow in a Turbine Blade Cascade", *J. Fluid Mech.*, Vol. 134, p85
- [5] Sieverding, C.H., 1984, "Recent Progress in the Understanding of basic Aspects of Secondary Flows in Turbine Blade Passages", *ASME Paper 84-GT-78*
- [6] Sharma, O.P., Butler, T.L., 1986, "Predictions of Endwall Losses and Secondary Flows in Axial Flow Turbine Cascades", *ASME Paper 86-GT-228*
- [7] Goldstein, R.J., Spores, R.A., 1988, "Turbulent Transport on the Endwall in the Region between Adjacent Turbine Blades", *ASME J. of Heat Transfer*, Vol. 110, pp. 862-869
- [8] Kawai, T., Shinoki, S., Adachi, T., 1988, "Visualization on Secondary Flow in a Turbine Cascade with and without Boundary Layer Fences", *Proc. 2nd Int. Symp. Fluid Control, Meas. Visual.*, pp 421
- [9] Schäffer, H., 1955, "Untersuchungen über die dreidimensionale Strömung durch axiale Schaufelgitter mit zylindrischen Schaufeln", PhD Thesis, TH Braunschweig, *Forsch. Ing.-Wes.* 21, pp. 9-19 and pp. 41-49
- [10] Hodson, H.P., Dominy, R.G., 1986, "The Off-Design Performance of a Low Pressure Turbine Cascade", *ASME Paper 86-GT-188*
- [11] Prümper, H., 1975, "Verbesserung des Wirkungsgrades axialer Turbinenstufen durch Reduzierung der Sekundärverluste", PhD Thesis, RWTH Aachen
- [12] Kawai, T., Shinoki, S., Adachi, T., 1989, "Secondary Flow Control and Loss Reduction in a Turbine Cascade using Endwall Fences", *JSME Int. Journal*, Series II, Vol. 32, No. 3, pp. 375
- [13] Dejc, M.E. et al., 1960, "Method of Increasing the Efficiency of Turbine Stages with Short Blades", *Teplotenergetika*, No. 2, Translation No. 2816, Associated Electrical Industries Ltd.
- [14] Harrison, S., 1990, "The Influence of Blade Lean on Turbine Losses", *ASME Paper 90-GT-55*
- [15] Jansen, M., Ulm, W., 1995, "Modern Blade Design for Improving Steam Turbine Efficiency", VDI Report No. 1185, pp. 277-290
- [16] Wang, Z., Han, W., 1995, "The Influence of Blade Negative Curving on the Endwall and Blade Surface Flows", *ASME Paper 95-GT-441*
- [17] Pioske, C., Gallus, H.E., 1997, "Dreidimensionale Turbinenbeschauelung", *Motorentechnische Zeitschrift* 58 (1997) 6, pp 358-362
- [18] Duden, A., Raab, I., Fottner, L., 1998, "Controlling the Secondary Flows in a Turbine Cascade by 3D Airfoil Design and Endwall Contouring", *ASME Paper 98-GT-72*
- [19] Haller, B.R., 1997, "Full 3D Turbine Blade Design", *VKI LS 1997-01 Secondary and Tip-Clearance Flows in Axial Turbines*
- [20] Denton, J.D., Wallis, A.M., Borthwick, D., Grant, J., Ritchey, I., 1996, "The Three-Dimensional Design of Low Aspect Ratio 50% Reaction Turbines", *IMEchE 1996*, S461/008, pp. 109-120
- [21] Chen, N.X., Zhou, Q., Huang, W., 1996, "A Study on Axial Skewing Effect of a Turbine Stator by 3D Navier-Stokes Analysis", *ASME-Paper 96-GT-149*
- [22] Sauer, H., Wolf, H., 1997, "Influencing the Secondary Flow in Turbine Cascades by the Modification of the Blade Leading Edge", *2nd European Conference on Turbomachinery*, Antwerp 1997
- [23] Morris, A.W.H., Hoare, R.G., 1975, "Secondary Loss Measurements in a Cascade of Turbine Blades with Meridional Wall Profiling", *ASME Paper 75-WA/GT-13*
- [24] Kopper, F.C., Milano, R., Vanco, M., 1981, "An Experimental Investigation of Endwall Profiling in a Turbine Blade Cascade", *AIAA Journal*, Vol. 19, No. 8, pp. 1033-1040
- [25] Ewen, J.S., Huber, F.W., Mitchell, J.P., 1973, "Investigation of the Aerodynamic Performance of Small Axial Turbines", *ASME Paper 73-GT-3*
- [26] Atkins, M.J., 1987, "Secondary Losses and End-Wall Profiling in a Turbine Cascade", *IMEchE Paper C255/87*
- [27] Rose, M.G., 1994, "Non-Axisymmetric Endwall Profiling in the HP NGV's of an Axial Flow Gas Turbine", *ASME Paper 249-GT-94*
- [28] Fritsch, G., Hoeger, M., Blaha, C., Bauer, D., 1997, "Viscous 3D Compressor Simulations on Parallel Architectures", *AIAA Paper 97-2876*
- [29] Wilcox, D.C., 1988, "Reassessment of the Scale Determining Equation for Advanced Turbulence Models", *AIAA Journal*, Vol. 25, No. 11, pp. 1299 – 1310
- [30] Gier, J., Ardey, S., Heisler, A., 2000, "Analysis of Complex Three-Dimensional Flow in a Three-Stage LP Turbine by means of Transitional Navier-Stokes Simulation", *ASME Paper 2000-GT-645*
- [31] Abu-Ghannam, B.J., Shaw, R., 1980, "Natural Transition of Boundary Layers – The Effects of Turbulence, Pressure Gradient and Flow History", *J. of Mechanical Engineering Science*, Vol. 22, No. 5, pp. 213 – 228
- [32] Drela, M., 1995, "Implementation of Modified Abu-Ghannam/Shaw Transition Criterion", MIT Aero-Astro
- [33] Gier, J., Ardey, S., 2001, "On the Impact of Blade Count Reduction on Aerodynamic Performance and Loss Generation in a Three-Stage LP Turbine", *ASME Paper 2001-GT-197*